Journal of Materials Chemistry B

RSC Publishing

PAPER

View Article Online
View Journal | View Issue

Published on 14 January 2013. Downloaded by Tufts University on 31/10/2014 18:10:31.

Cite this: J. Mater. Chem. B, 2013, 1, 1614

Self-assembly of polyion complex nanocarriers from ammonium glycyrrhizinate and monomethoxy poly(ethylene glycol)-*b*-poly(γ-amino-ε-caprolactone)

Yan Zhang,*[a] Jianjing Liu,[a] Yutong Fu,[a] Ke Tan,[b] Zhaoyang Ye[b] and Meidong Lang*[a]

Received 29th October 2012
Accepted 14th January 2013

DOI: 10.1039/c3tb00012e

www.rsc.org/MaterialsB

A novel polyion complex (PIC) drug carrier was developed *via* electrostatic self-assembly in aqueous media based on our previous copolymer methoxy poly(ethylene glycol)-*b*-poly(γ-amino-ε-caprolactone) (mPEG-*b*-PACL) and anti-hepatotoxic drug ammonium glycyrrhizinate (AMG). The formation and the physicochemical properties of the polyion complex nanoparticles in aqueous solution were investigated by various methods. The results demonstrated that AMG was encapsulated successfully and the nanoparticles had a core–shell or tri-layer spherical structure based on the length of the PACL. The AMG/PACL PIC also displayed a high loading capacity and encapsulation efficiency of up to 41.8% and 91.7%, respectively. Furthermore, the nanoparticles enabled a continuous and sustained *in vitro* AMG release and the release half time was about 3 times that of the free AMG's. Results obtained by 3-(4,5-dimethylthiazol-2-yl)-2,5-diphenyl tetrazolium bromide (MTT) assay, flow cytometry and fluorescence microscopy revealed that AMG loaded nanoparticles demonstrated greater prevention of liver cell apoptosis induced by lipopolysaccharide (LPS). These findings indicated that methoxy poly(ethylene glycol) (mPEG)-*b*-poly(γ-amino-ε-caprolactone) could be an efficient AMG carrier and could even be used as a delivery template for some other negatively charged water-soluble drugs or gene delivery systems.

Introduction

Polyion complex (PIC) nanoparticles, which arise from the electrostatic interactions of double hydrophilic block ionomers with oppositely charged species, have been a widely researched topic for various applications,[1–3] especially for delivery of low molecular weight drugs, siRNA and so on.[4,5] Such drug delivery systems are spontaneously formed in aqueous solutions and avoid complicated syntheses and the use of organic solvents, which could eliminate side-effects caused by residual solvents.[6] Also, PIC nanoparticles could overcome the biological hurdles limiting the delivery of nucleic acids, enzymes and some charged drugs.[7] The simplicity of their design and their availability for preparation make them potential candidates in pharmaceutical and biomedical fields.[8–10]

Poly(ε-caprolactone) (PCL) is one of the most extensively studied synthetic biodegradable polymers in various formulations for drug delivery.[11–13] However, the hydrophobicity of PCL is the major drawback responsible for its limited use in polyion complex micelle carriers, thus the investigation of functionalized PCL has attracted great interest. For example, poly(γ-bromo-ε-caprolactone-*co*-caprolactone) was synthesized with a statistical and blocky structure, and the bromide pendant groups were quaternized by pyridine, and further used to condense DNA. However, a dose-dependent cytotoxicity was observed with increasing concentration of the copolymer due to the presence of pyridinium groups.[14] In our previous report, we have reported the biodegradable cationic monomethoxy poly(ethylene glycol)-*b*-poly(γ-amino-ε-caprolactone), which was not cytotoxic until the concentration reached 500 mg L^{-1}. Moreover, it is unique in that the pendant amino groups in each repeating unit are positively charged which could impart water-solubility to the polymer .[15]

Ammonium glycyrrhizinate (AMG) is a derivative of glycyrrhizinate and has improved aqueous solubility. The pharmacologically active form of AMG is glycyrrhetic acid (GA), obtained by metabolism *in vivo*, which endows various pharmacological effects such as anti-inflammatory properties, anti-allergic disorder effects and the therapeutic effect for viral diseases such as chronic hepatitis.[16–19] However, GA could cause side-effects such as hypertension, edema and electrolyte disturbances. Thus, the GA drug delivery system attracted great interest to solve such problems.[20]

Glycyrrhizinate-loaded carriers have been reported by many groups. For example, glycyrrhetic acid was encapsulated into poly(DL-lactic acid-*co*-glycolic acid) by a solvent evaporation

[a]Shanghai Key Laboratory of Advanced Polymeric Materials, Key Laboratory for Ultrafine Materials of Ministry of Education, School of Materials Science and Engineering, East China University of Science and Technology, Shanghai 200237, China. E-mail: zhang_yan@ecust.edu.cn; mdlang@ecust.edu.cn; Fax: +86-21-64251764; +86-21-64253916; Tel: +86-21-64251764; +86-21-64253916

[b]State Key Laboratory of Bioreactor Engineering, School of Bioengineering, East China University of Science and Technology, Shanghai, 200237, China

This journal is © The Royal Society of Chemistry 2013

Published on 14 January 2013. Downloaded by Tufts University on 31/10/2014 18:10:31.

method.[20] M. Carafa *et al.* used the niosomes made up of surfactants and cholesterol to load ammonium glycyrrhizinate.[21] Chitosan and poly-L-lysine were widely used as cationic materials to incorporate the glycyrrhetic acid by electrostatic interaction. However, either their biological properties lacked supporting data or the preparation process has not been studied thoroughly.[22–25]

Herein, we used cationic monomethoxy poly(ethylene glycol)-*b*-poly(γ-amino-ε-caprolactone) and anionic drug ammonium glycyrrhizinate to prepare the polyion complex nanocarriers. The cationic poly(γ-amino-ε-caprolactone) and ammonium glycyrrhizinate could form finite sized complexes composed of a dense polyelectrolyte core and a swollen PEG corona that stabilized the nanostructure in aqueous dispersion and protected the core from aggregation by steric repulsion. The *in vitro* drug release and the effect of protecting liver cells from apoptosis induced by lipopolysaccharide (LPS) were examined to assess their potential as AMG carriers. Overall, the results further advance the potential use of mPEG-*b*-PACL for other ionic drugs and genes.

Experimental

1 Materials and methods

1.1 Materials. Methoxy poly(ethylene glycol ($M_n = 2000$ Da, mPEG) was purchased from Aldrich (Milwaukee, WI, USA) and further dried by azeotropic distillation with anhydrous toluene prior to use. mPEG-*b*-PACL block copolymer was synthesized as described in our previous report.[15] The number of repeating units for mPEG was 45, and the samples were named P-A1–P-A5 according to the length of the PACL blocks (Table 1). Ammonium glycyrrhizinate (AMG, 97%) was bought from Aladdin and used as received without further purification. Cell culture media Rosewell Park Memorial Institute (RPMI 1640) and phosphate buffered saline (PBS) were supplied by Invitrogen (CA, USA). Lipopolysaccharide (LPS, *Escherichia coli*, 0111B4) was obtained from Sigma. Albumin kit (Alb, 100 tube/96 samples) and lactate dehydrogenase kit (LDH, 100 tube/48 samples) were both obtained from Nanjing Jiancheng Bioengineering Institute. 3-(4,5-Dimethylthiazolyl-2)-2,5-diphenyl tetrazolium bromide (MTT) was provided by Sigma. HepG2 liver carcinoma cells were supplied by School of Biotechnology, East China University of Science and Technology. All other commercially available reagents and solvents were used without further purification unless otherwise mentioned.

Table 1 Effect of the chain length of PACL on the mean particle size and zeta potential of the AMG-loaded nanoparticles at a weight ratio of $W_{AMG}/W_{PACL} = 0.25$

Sample[a]	Polymer M_n[b](kDa)	DP[c]	D_h (nm)	Zeta potential (mV)
P-A1	3.4	12	120	1.1
P-A2	5.1	26	149	8.7
P-A3	8.5	55	153	12.3
P-A4	10.2	69	188	28.1
P-A5	11.3	79	203	29.8

[a] Five samples of mPEG-*b*-PACL with different polymer compositions were synthesized, and AMG-loaded nanoparticles were prepared and denoted as P-A1, P-A2, P-A3, P-A4 and P-A5, accordingly. [b] Calculated using ^{1}H NMR (D_2O as solvent). [c] Degree of polymerization.

1.2 Preparation of AMG-loaded nanoparticles. The AMG-loaded nanoparticles were prepared by electrostatic assembly between positively charged mPEG-*b*-PACL and negatively charged AMG at room temperature. Typically, given amounts of mPEG-*b*-PACL were dissolved in double-distilled water at a concentration of 2.0 mg mL^{-1} and stirred for 2 h, after which the final pH of the solution was adjusted to 4 by the addition of small amounts of NaOH or HCl as necessary. Meanwhile, AMG was dissolved in double-distilled water at a concentration of 1.0 mg mL^{-1} and stirred for 2 h. Both solutions were purified by passing through 0.45 μm syringe filters to remove dust. Under gentle stirring, 5 mL AMG solution was added drop-wise to 5 mL mPEG-*b*-PACL solution. The mixture was stirred for 2 h to ensure full complexation between mPEG-*b*-PACL and AMG at room temperature. After that, an opalescent suspension of nanoparticles was formed.

The solid complex aggregates were prepared by a centrifugation method. Briefly, the AMG-loaded aqueous suspension was further filtered through a 0.45 μm syringe filter to remove the AMG impurities. Then the AMG-loaded aqueous suspension was ultra centrifugated at 150 000*g* at 20 °C for 2 h to get rid of the free AMG. The residue was redispersed with double-distilled water and separated by ultra centrifugation twice. The precipitate was frozen and lyophilized to obtain dried AMG-loaded nanoparticles.

1.3 *In vitro* drug release. The *in vitro* release profiles of AMG from AMG-loaded nanoparticles were studied using the membrane diffusion technique. Typically, 4.5 mg dried AMG and AMG-loaded nanoparticles were dispersed in 5 mL PBS (pH 7.4) and placed in a dialysis tube (MWCO 3500), respectively. The dialysis bag was directly immersed in 55 mL PBS (pH 7.4), and incubated at 37 °C in a shaking bath (HZQ-F160, Taicang Experiment Factory, Jiangsu Province, China) at a constant stirring rate (100 rpm). At predetermined time intervals, 5 mL PBS was withdrawn from the release medium, and an equivalent volume of fresh PBS solution was added to the medium. According to the standard curve of AMG solution in PBS (pH 7.4), the amount of AMG in the release system was analyzed by a UV/Vis spectrometer at a wavelength of 257 nm. The cumulative release was calculated using the following equation:

$$\text{Cumulative release } (\%) = \frac{60.0C_n + 5.0\sum C_{n-1}}{W_0} \times 100\% \quad (1)$$

where W_0 (mg) is the weight of AMG in the AMG-loaded nanoparticles. C_n and C_{n-1} (mg mL^{-1}) are the concentrations of AMG in the PBS which was withdrawn n and $n-1$ ($n > 0$) times, respectively.

1.4 *In vitro* cell experiments

1.4.1 Cell culture. Human HepG2 cells were maintained in RPMI 1640 culture medium, supplemented with 10% fetal bovine serum (FBS), 100 U mL^{-1} penicillin, and 100 mg L^{-1} of streptomycin. The cells were cultured at 37 °C in a humidified atmosphere containing 95% air and 5% CO_2.

Published on 14 January 2013. Downloaded by Tufts University on 31/10/2014 18:10:31.

1.4.2 The effect on inhibiting liver cell apoptosis induced by lipopolysaccharide

(1) Cell viability. For MTT assay, the HepG2 cells were seeded at a density of 1×10^4 cells per well in a 96-well microassay plate and incubated for 24 h to permit cell attachment. Subsequently, the cells were incubated in RPMI 1640 culture medium containing (a) free lipopolysaccharide (LPS), (b) mPEG-*b*-PACL (DP = 12) and LPS, (c) culture medium (without LPS), (d) free AMG and LPS and (e) AMG-loaded nanoparticles and LPS. All the samples were filtered through a 0.22 μm microfilter and diluted with RPMI 1640 to obtain pre-set concentrations. The concentration of LPS was fixed at 20 μg mL^{-1} for each sample. The cells were incubated for an additional 24 h at 37 °C in a 5% CO_2 incubator. The culture medium was then replaced with fresh RPMI 1640 (200 μL) followed by the addition of 20 μL of 5 mg mL^{-1} MTT solution in PBS and the cells were incubated for an additional 4 h at 37 °C. The MTT-containing medium was removed and 200 μL of DMSO was added to solubilize the formazan products with gentle agitation for 10 min. Absorbance was measured at 570 nm using a microplate reader (Bio-Rad 550) to determine the optical density (OD_{570}) value.

$$\text{Cell viability (\%)} = (OD_{treated}/OD_{control}) \times 100\% \quad (2)$$

where $OD_{treated}$ was obtained for the cells treated by various samples mentioned above, $OD_{control}$ was obtained for the cells treated only by RPMI 1640 culture medium, and the other culture conditions were the same. The data are given as mean +/− standard deviation (SD) based on three independent measurements.

(2) Flow cytometry and fluorescence microscopy. The cells were seeded at a density of 4×10^5 cells per well in 6-well plates and cultured for 24 h in RPMI 1640 culture medium. Thereafter, the cells were incubated in the culture medium containing (I) free lipopolysaccharide (LPS), (II) free AMG and LPS, (III) AMG-loaded nanoparticles and LPS and (IV) culture medium (without LPS) for another 24 h. The concentration of LPS was 20 μg mL^{-1} and that of AMG was 1 mg mL^{-1}. The cells were washed with PBS three times and harvested with trypsinization without ethylene diamine tetraacetic acid (EDTA). The cell pellets were redispersed in a fixing buffer (FACS buffer with 1% formaldehyde), followed by fixation and double-staining with Annexin V-fluorescein isothiocyanate (Annexin V-FITC) and propidium iodide (PI). The cells were kept in the dark for 15 min and transferred to FACS tubes. Flow cytometry was performed using a BD FACS Calibur TM (BD Bioscience Immunocytometry Systems, CA, USA). The data were analyzed by Cell Quest software and are given as mean +/− standard deviation (SD) based on four independent measurements.

For the fluorescence study, HepG2 cells were seeded at a density of 1×10^5 cells per well in 6-well plates. Other processing procedures were performed as described above. The harvested HepG2 cells were washed twice with PBS and fixed with 1.5 mL 3.7% paraformaldehyde for 30 min at room temperature. They were then stained with 100 μL 4′,6-diamidino-2-phenylindole (DAPI) and kept in the dark for 30 min at 4 °C until observation. The nuclei states of HepG2 cells were verified by a fluorescence microscope (Ecl IPSE Ti-s Nikon).

(3) Measurement of albumin (Alb) and lactate dehydrogenase (LDH). The albumin and lactate dehydrogenase levels secreted by HepG2 cells were measured by Alb and LDH kits according to the manufacturer's instructions. Based on the cells cultured in the flow cytometry assay, the supernatants were collected to analyze the albumin and lactate dehydrogenase concentrations on a microplate reader (Sunrise remote Tecan) at the pre-set time intervals.

2 Characterization

2.1 The formation of the AMG-loaded nanoparticles. UV-vis spectra were recorded on a UV-vis spectrophotometer (UV-vis 8500 Techcomp, China) in the range of wavenumbers between 200 nm and 400 nm to confirm the complex formation between mPEG-*b*-PACL and AMG.

The steady-state fluorescence spectroscopy measurements were performed on a fluorescence spectrophotometer (Horiba Jobin Yvon, Inc.) to evaluate the complexation process of mPEG-*b*-PACL (DP = 12) and AMG. A pyrene solubilization method was used to detect the onset of nanoaggregates. A pre-determined amount of pyrene in acetone was added to the vials, followed by acetone evaporation. Afterwards, aqueous solutions containing a known mass of nanoparticles with different weight ratios of AMG to PACL were added and left to equilibrate in an incubator overnight at 37 °C. The final pyrene concentration was kept at 6.0×10^{-7} mol L^{-1}. The excitation spectra were scanned from 200 to 360 nm at a fixed emission wavelength of 372 nm with a bandwidth of 3 nm. All measurements were performed at room temperature. The fluorescence intensity ratios of pyrene (I_{337}/I_{333}) were calculated and plotted against the weight ratios of AMG to PACL.

Optical transmittance of the aqueous mPEG-*b*-PACL (DP = 69)/AMG solutions at various weight ratios were measured at a wavelength of 546 nm with a UV-vis spectrometer (UV-vis 8500 Techcomp, China). The data were given as the average value based on three independent measurements.

2.2 Particle size and morphology of the AMG-loaded nanoparticles. The particle size and size distribution of the AMG-loaded nanoparticles prepared at various PACL lengths or weight ratios were determined by dynamic light scattering (DLS). The mean particle diameter of the nanoparticles was studied on a Malvern Nano-ZS90 spectrogoniometer (Malvern instruments Ltd, Worcestershire, UK) equipped with a 532 nm argon laser and 90° detection optics. The samples (1 mg mL^{-1}) were passed through a 0.45 μm microfilter before measurement to remove large aggregates.

The zeta potentials of the AMG-loaded nanoparticles obtained at various PACL lengths and weight ratios were measured by a laser Doppler electrophoresis technique using a Malvern Nano-ZS. The zeta potentials were based on three independent measurements at 25 °C.

The morphologies of AMG-loaded nanoparticles prepared from different PACL lengths at a fixed weight ratio of 0.25 were observed on a TEM instrument (JEOL/JEM-2000EXII) operated

 This journal is © The Royal Society of Chemistry 2013

Published on 14 January 2013. Downloaded by Tufts University on 31/10/2014 18:10:31.

at an accelerating voltage of 60 keV. The samples were prepared by dropping solution (1 mg mL^{-1}) on a copper grid coated with carbon film and allowed to dry at room temperature.

2.3 Investigation of drug loading capacity (DLC) and encapsulation efficiency (EE). After the AMG-loaded nanoparticles were separated by ultra centrifugation, the centrifugal solution containing free AMG was collected to determine the amount of free AMG and the drug loading capacity and encapsulation efficiency were obtained accordingly. The absorbance of free AMG at 257 nm was measured on a UV-vis spectrophotometer (UV-vis 8500 Techcomp, China). The weight of free AMG was calculated with a standard curve obtained from AMG/H_2O solutions at a series of AMG concentrations. The amount of AMG in the nanoparticles was obtained by subtracting the free AMG in the supernatant from the total AMG, and the DLC and EE were calculated as shown in eqn (3) and (4):

$$\text{DLC}\ (\%) = \frac{\text{The amount of AMG in the nanoparticles}}{\text{Total amount of the nanoparticles}} \times 100\% \quad (3)$$

$$\text{EE}\ (\%) = \frac{\text{The amount of AMG in the nanoparticles}}{\text{Total amount of AMG}} \times 100\% \quad (4)$$

Results and discussion

1 Formation of the AMG-loaded nanoparticles

Cationic mPEG-*b*-PACL copolymers have been synthesized and exhibit different solution behaviors based on the length of PACL.[15] As seen from Scheme 1, the carboxyl groups endow ammonium glycyrrhizinate with a negative charge and the amino groups in mPEG-*b*-PACL produce positive properties accordingly. The interaction between mPEG-*b*-PACL and ammonium glycyrrhizinate resulted in the formation of the PIC nanoparticles. Based on our preliminary results, the zeta potential of mPEG-*b*-PACL at pH = 4 had a maximum value throughout the whole pH range (data not shown), thus the complexation of mPEG-*b*-PACL with AMG was conducted at pH 4. The obtained nanoparticle solution remained transparent for two weeks and no obvious precipitation was observed, which revealed a high storage stability of the nanoparticles.

The complexation between mPEG-*b*-PACL and AMG was confirmed by UV spectroscopy. Fig. 1 shows the UV spectra of free AMG (a), mPEG-*b*-PACL (b) and AMG-loaded nanoparticles (c). As seen from Fig. 1(a), the maximum absorption peak of AMG was at a wavelength of 257 nm, while there was no absorption here in Fig. 1(b) for mPEG-*b*-PACL. However, there was an obvious blue shift in Fig. 1(c), which was attributed to the complexation that occurred, and the absorption of the AMG varied. However, FT-IR confirmed the mPEG-*b*-PACL structure in the AMG loaded nanoparticle spectrum (data not shown).

As found in our previous study, mPEG-*b*-PACL exists from unimers to core–shell micelles when the DP (Degree of Polymerization) of PACL varied from 26 to 36. The interactions between mPEG-*b*-PACL (unimers) and AMG was further confirmed by steady-state fluorescence studies using pyrene as a probe and by transmittance tests. The ratio of intensities of the excitation energy in the pyrene spectrum (I_{337}/I_{333}) correlated well with the solvent polarity and served as a measure of the polarity of the environment.[26,27] The interactions between the cationic polyion and the negatively charged AMG could lead to the formation of a hydrophobic microphase. Fig. 2(a) shows the fluorescence spectra of the PIC nanoparticles at different W_{AMG}/W_{PACL} ratios of mPEG-*b*-PACL (DP = 12). The I_{337}/I_{333} ratio remained constant or only slightly changed below the critical association concentration (cac), which was attributed to the weak interactions between PACL and AMG. While above the cac, the interactions between AMG and mPEG-*b*-PACL increased and led to a sharp increase in the I_{337}/I_{333} ratio, which reflected the partitioning of pyrene into the hydrophobic environment. Fig. 2(b) shows the variation of the optical transmittance of the mPEG-*b*-PACL (DP = 69) and AMG system. The mPEG-*b*-PACL (DP = 69) has already formed the core–shell micelles when it dispersed in the water due to the hydrophobicity of the PACL chain. The amino groups would move to the core–shell interface and impart a positive surface. Thus the negative AMG interacted with them by electroelectric interactions. It was seen from Fig. 2(b) that the optical transmittance decreased as the weight ratio of mPEG-*b*-PACL to AMG (W_{AMG}/W_{PACL}) increased, which confirmed that the AMG loaded nanoparticles formed.

Here, it was deduced that there existed two kinds of mechanism for the drug encapsulation process by mPEG-*b*-PACL. A schematic presentation of the complexation behavior is proposed in Scheme 2. The core–shell nanoparticles were formed *via* complexation of AMG and a single chain of mPEG-*b*-PACL when the chain length of mPEG-*b*-PACL was below the critical length (Lc, DP from 26 to 36), while tri-layer nanoparticles were obtained due to the cationic amino groups

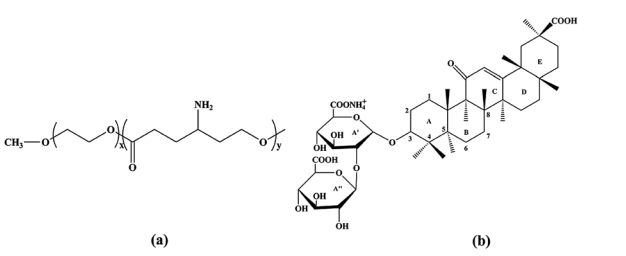

Scheme 1 The structures of (a) the mPEG-*b*-PACL copolymer and (b) ammonium glycyrrhizinate.

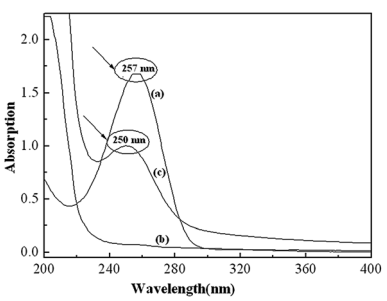

Fig. 1 The UV absorption of AMG (a), mPEG-*b*-PACL (DP = 12) (b) and P-A1 (c).

Published on 14 January 2013. Downloaded by Tufts University on 31/10/2014 18:10:31.

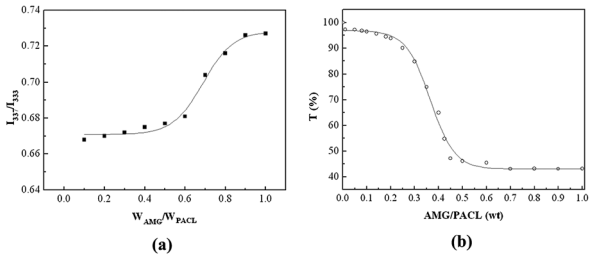

Fig. 2 Plot of the fluorescence intensity ratios, I_{337}/I_{333}, *versus* weight ratios of W_{AMG}/W_{PACL} at room temperature, the sample was mPEG-*b*-PACL (DP = 12)/AMG (a) optical transmittance of mPEG-*b*-PACL (DP = 69)/AMG nanoparticles (b).

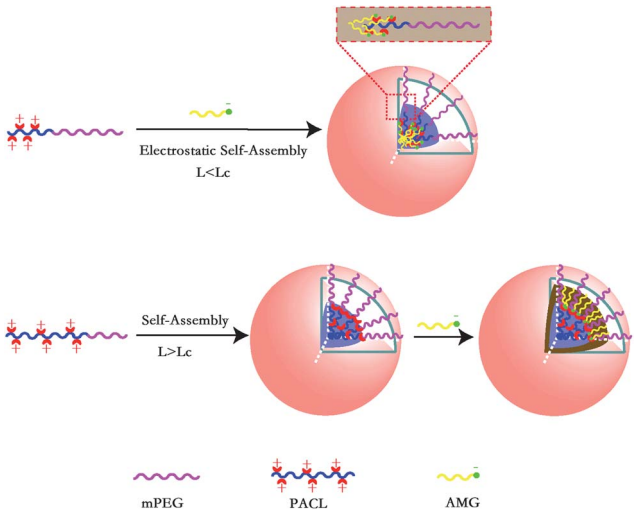

Scheme 2 Schematic presentation of the different complexation behaviors of mPE-*b*-PACL and AMG in aqueous solution.

situated at the interface of the nanoparticles and the anion AMG interacted with them when the chain length of mPEG-*b*-PACL was above the Lc.

2 Particle size and morphology of the AMG-loaded nanoparticles

AMG-loaded nanoparticles were prepared at various PACL lengths and different weight ratios of W_{AMG}/W_{PACL}. The size and surface charge of the nanoparticles were further investigated. Table 1 summarizes the effect of PACL chain length on the mean particle sizes and zeta potentials. At elevated chain lengths, both $\langle D_h \rangle$ and the zeta potential increased dramatically at a certain weight ratio of 0.25. Moreover, it was seen from Fig. 3 that the D_h increased regularly with an increase of the weight ratio of AMG to PACL. For example, the average diameter of mPEG-*b*-PACL (DP = 12) serial nanoparticles was in the range of 8–173 nm when the weight ratio increased from 0 to 0.4 (Fig. 3(a)), while it appeared that the size of mPEG-*b*-PACL (DP = 69) serial nanoparticles (152–282 nm) (Fig. 3(b)) were much larger than those of mPEG-*b*-PACL (DP = 12) serial nanoparticles. One reasonable explanation was that the mPEG-*b*-PACL (DP = 69) has formed core–shell nanoaggregates due to

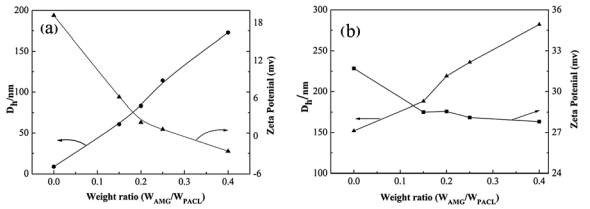

Fig. 3 The mean particle sizes and zeta potential measurements of different types of AMG-loaded nanoparticles: (a) mPEG-*b*-PACL (DP = 12) serial nanoparticles; and (b) mPEG-*b*-PACL (DP = 69) serial nanoparticles.

the long length of PACL before complexation with AMG, then the charged amino groups on the interface interacted with the negative AMG, which led to the formation of tri-layered nanoparticles, and the obtained AMG-loaded nanoparticles were relatively loose; the other explanation may be that the longer chain length of PACL endowed it with an increase in positive charge and led to greater AMG interactions with mPEG-*b*-PACL.

Further information on the drug-loaded nanoparticles was collected from the zeta potential analysis. Representative experimental results are also shown in Fig. 3. Unlike the results obtained in the D_h, the zeta potentials decreased significantly with the increase in the weight ratio of AMG to mPEG-*b*-PACL, which was attributed to the neutralization between the carboxyl groups in AMG and the amino groups in mPEG-*b*-PACL with the addition of AMG solution into the mPEG-*b*-PACL solution. Obviously, the zeta potential of mPEG-*b*-PACL (DP = 69) (31.7–27.8 mV, Fig. 3(b)) nanoparticles was larger than that of mPEG-*b*-PACL (DP = 12) serial nanoparticles (19.2 to −2.41 mV, Fig. 3(a)), which was also in excellent agreement with the results obtained in particle size studies and could give a reasonable explanation.

To gain more insight into the complexation behavior of the AMG-loaded nanoparticles, the detailed morphologies have been analyzed by TEM. Fig. 4 shows the TEM images of AMG-loaded nanoparticles, which were formed in aqueous solution at a weight ratio of 0.25. Well-defined spherical shaped P-A1 (Fig. 4(a)) and P-A4 (Fig. 4(b)) nanoparticles can be observed and the mean particle sizes were around 100 nm and 150 nm.

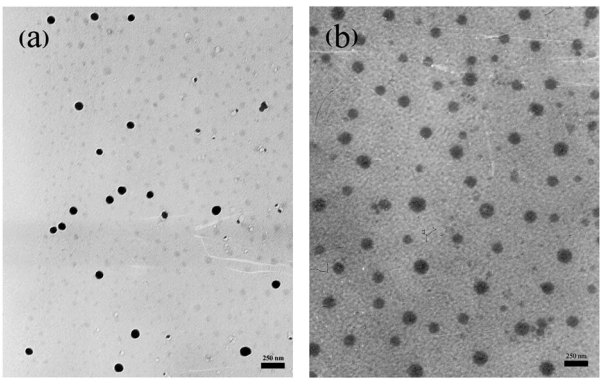

Fig. 4 The TEM images of different types of AMG-loaded nanoparticles: (a) P-A1; and (b) P-A2.

This journal is © The Royal Society of Chemistry 2013

Published on 14 January 2013. Downloaded by Tufts University on 31/10/2014 18:10:31.

Taking into account the hydration and polydispersity effects, the particle sizes by TEM were in good agreement with the data obtained from DLS.

3 Investigation of drug loading capacity and encapsulation efficiency

Fig. 5 shows the drug loading capacity and encapsulation efficiency *vs.* weight ratio of AMG-loaded nanoparticles. According to the results, along with the increase of weight ratio, the drug loading capacity of mPEG-*b*-PACL (DP = 12) serial nanoparticles (11.2–20.6%) and mPEG-*b*-PACL (DP = 69) (20.2–41.8%) serial nanoparticles increased, and the DLC of mPEG-*b*-PACL (DP = 12) serial nanoparticles were markedly lower than those of mPEG-*b*-PACL (DP = 69) serial nanoparticles. Meanwhile, the encapsulation efficiency decreased for mPEG-*b*-PACL (DP = 12) serial nanoparticles (86–71.9%) and mPEG-*b*-PACL (DP = 69) serial nanoparticles (91.7–58.6%) accordingly. As mentioned above, the mechanism of AMG association to PACL nanoparticles was mediated by ionic interactions between the carboxyl groups in AMG and the amino groups in mPEG-*b*-PACL. These differences may derive from the charges of mPEG-*b*-PACL and the different ways of embedding. A bold hypothesis was that the AMG-loaded nanoparticles formed in the second mechanism were enriched with AMG.

4 *In vitro* drug release behavior of AMG-loaded nanoparticles

The *in vitro* release of free-AMG and AMG-loaded nanoparticles was monitored in PBS (pH 7.4) at 37 °C. Fig. 6 displays the release profile of AMG from AMG-loaded nanoparticles. A vivid phenomenon was that free-AMG showed a rapid release with almost 50% initial burst release in the first 5 h, which demonstrated that the dialysis bag had almost no effect on the speed of release of the drug. The release of AMG was almost complete within 18 h (*i.e.* 99%). It was obvious that the AMG-loaded nanoparticles presented a sustained release, and the drug release ratio was in relation to the compositions of mPEG-*b*-PACL. There was no obvious rapid initial burst and the cumulative releases of P-A1 and P-A4 were 50% and 40%, respectively during the first 12 h. Up to 48 h, approximately 92% and 88% drug was released for P-A1 and P-A4, followed by a slow drug release rate until release was complete. In addition, in the embedded figure, it could be found that the release half lives of P-A1 and P-A4 were 12 h and 16 h, respectively, while it was only 5 h for pure AMG. As for the difference between P-A1 and P-A4,

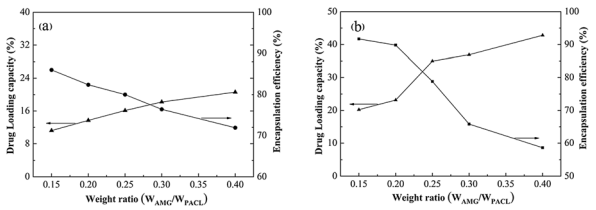

Fig. 5 The drug loading capacities and encapsulation efficiencies of different types of AMG-loaded nanoparticles: (a) mPEG-*b*-PACL (DP = 12) serial nanoparticles; and (b) mPEG-*b*-PACL (DP = 69) nanoparticles.

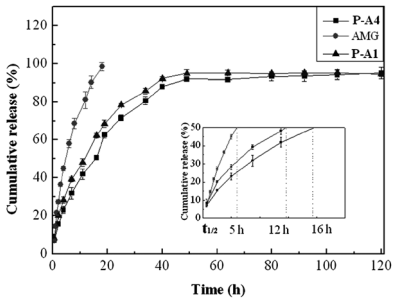

Fig. 6 Typical *in vitro* release profiles of pure AMG and different types of AMG-loaded nanoparticles, the weight ratio of the nanoparticles was 0.25.

the structure of the P-A1 nanoparticles disassociated while the P-A4 still existed as core–shell micelles as the release proceeded, which maybe caused the release from P-A4 to slow down. Based on the data collected, we could draw the conclusion that the effect of mPEG-*b*-PACL encapsulation on AMG release was obvious and the AMG-PACL nanoparticle system might be used to provide continuous release.

5 The effect on inhibiting liver cell apoptosis induced by lipopolysaccharide

Based on previous findings in the literature, abnormal apoptosis of liver cells could be induced by lipopolysaccharide (LPS), TNF α or actinomycin D (Act D) and so on, which are closely related to the onset of various acute and chronic liver diseases.[28,29] Glycyrrhizinate, which was extracted from glycyrrhiza, showed strong effects on protecting liver cell membranes and improving liver function.[30,31] In this research, HepG2 hepatoma cells, the biological characteristics of which are similar to those of normal liver cells, were used as the model cells to evaluate the effect of pure AMG and AMG-loaded nanoparticles (P-A1 nanoparticles were used) to prevent liver cell apoptosis induced by lipopolysaccharide (LPS).

To assess cytotoxicity, the cell viability was evaluated by MTT assay. The results demonstrated that cells treated with free LPS

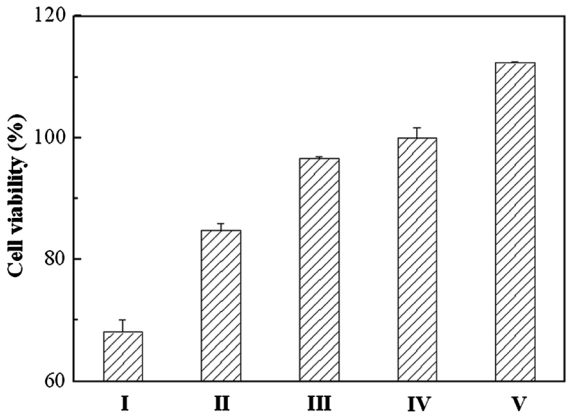

Fig. 7 Cell viability of HepG2 cells treated with different samples of free lipopolysaccharide (LPS) (I); mPEG-*b*-PACL (with LPS) (II); free AMG with LPS (III); culture medium (without LPS) (IV) and PA-1with LPS (V).

Published on 14 January 2013. Downloaded by Tufts University on 31/10/2014 18:10:31.

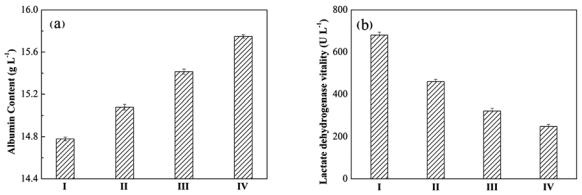

Fig. 8 Albumin secretion (a) and lactate dehydrogenase (b) of HepG2 cells in supernatant of the cell medium treated with different samples: (I) free lipopolysaccharide (LPS); (II) culture medium (without LPS); (III) free AMG and LPS and (IV) AMG-loaded nanoparticles and LPS.

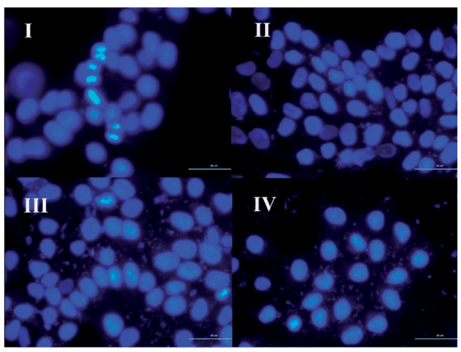

Fig. 9 Fluorescence microscope images of HepG2 cells in the supernatant of cell medium treated with different samples: (I) free lipopolysaccharide (LPS); (II) free AMG and LPS; (III) AMG-loaded nanoparticles and LPS and (IV) culture medium (without LPS).

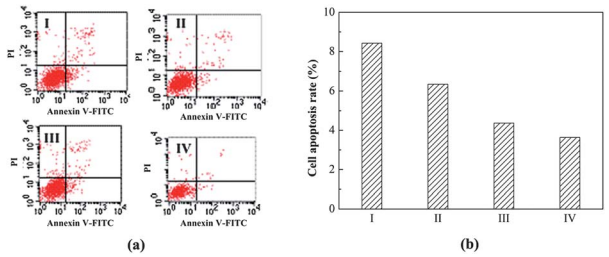

Fig. 10 Apoptosis of HepG2 cells in the supernatant of cell medium treated with different samples: (I) free lipopolysaccharide (LPS); (II) free AMG and LPS; (III) AMG-loaded nanoparticles and LPS and (IV) culture medium (without LPS).

(Fig. 7(I)) exhibited cytotoxicity to HepG2 cells after 24 h, which indicated LPS could induce apoptosis to a certain extent. The empty mPEG-*b*-PACL (DP = 12) nanoparticles with free LPS also have induced apoptosis due to LPS (Fig. 7(II)). The viability of HepG2 cells (Fig. 7(III)) in the presence of free AMG solution and LPS is enhanced in comparision with (Fig. 7(II)).

Above all, HepG2 cells treated with AMG-loaded nanoparticles and LPS (Fig. 7(V)) showed the highest cell viability among the groups. Therefore, AMG-loaded nanoparticles had a better effect on inhibiting liver cell apoptosis induced by LPS in comparision with inhibition of apoptosis by AMG and LPS.

Albumin is a mature albumen secreted by liver and HepG2 cells, which could be used as the labeled protein of the HepG2 cell differentiation.[32] The levels of albumin secretion in the supernatant of HepG2 cell culture are shown in Fig. 8(a). Those cell aggregations treated with free LPS secreted the least albumin into the medium. Obviously, albumin secretion of HepG2 treated with free AMG with LPS (Fig. 8(a)III) was much more than LPS and the control (Fig. 8(a)I and II), which indicated that the AMG could protect the cells from abnormal apoptosis and promote the secretion of albumin to a certain degree. Moreover, the AMG loaded nanoparticles had the highest albumin secretion levels (Fig. 8(a)IV). These results were in good agreement with the cell viability results.

Lactate dehydrogenase (LDH) exists in the cell slurry and is released when cell necrosis takes place, and the amount of LDH represents the cell necrosis degree.[33] In Fig. 8(b), compared with the control (II), it revealed that LPS treatment (I) induced a significant increase in the lactate dehydrogenase secretion. The cells treated with AMG and LPS (III) and AMG-loaded nanoparticles with LPS treatment (IV) had relatively lower secretion levels. These results are also in accordance with that of albumin secretion, which further confirmed the AMG loaded nanoparticles had a better effect on inhibiting HepG2 cells apoptosis.

In apoptotic cells, mitochondria lose their membrane integrity which results in a loss of mitochondrial membrane potential.[34] In order to determine whether mitochondrial changes occurred in the HepG2 cells treated with different culture media fluorescence microscopy was employed. Compared with the control (Fig. 9(IV)), the regular cells and some fragmentation (white dots) coexisted in Fig. 9(I), while the HepG2 cells treated with free AMG with LPS (II) and AMG-loaded nanoparticles with LPS (III)) remained intact and regular without fragamentation (Fig. 9(II) and (III)), indicating that the mitochondria invoked no obvious changes. These results suggested that AMG-loaded nanoparticles could inhibit the effects of LPS on cells apoptosis.

In order to evaluate the HepG2 cells apoptosis status intuitively, we performed the cells apoptosis assay by flow cytometry (Fig. 10(a)). The AMG-loaded nanoparticles were the best at preventing cell apoptosis and the cell apoptosis rate of HepG2 cells could be calculated according to Fig. 10(a). It was seen from Fig. 10(b) that the cell apoptosis rate of HepG2 cells treated by LPS (Fig. 10(b)I, 8.43%) was significantly higher than the others (Fig. 10(b)II–IV, 6.35%, 4.37% and 3.64%, respectively), and AMG-loaded nanoparticles inhibited cell apoptosis greatly, which indicated that AMG-loaded nanoparticles would play an important role in liver cell protection.

Conclusion

Herein, effective PIC nanocarriers based on mPEG-*b*-PACL and AMG were successfully obtained in aqueous media by electrostatic assembly. Two kinds of mechanism were adopted to elucidate the complexation process according to the chain length-dependence properties of mPEG-*b*-PACL. The PIC nanoparticles were on the nanoscale and had sustained release behavior. Moreover, the *in vitro* cell experiments demonstrated that AMG-loaded nanoparticles had a better effect on preventing liver cell apoptosis induced by LPS. It is also expected that this polymer system could be used as a template for other

 This journal is © The Royal Society of Chemistry 2013

anionic drugs or gene carrier systems, and the relevant work is in progress.

Acknowledgements

Financial support from the National Natural Science Foundation of China (20804015, 31000424), the Fundamental Research Funds for the Central Universities (WD0913008, WD1014036), Shanghai Key Laboratory Project (08DZ2230500) is gratefully acknowledged. Authors would like to thank Dr Alicia Potuck for her critical reading.

Published on 14 January 2013. Downloaded by Tufts University on 31/10/2014 18:10:31.

Notes and references

1 M. Stepanek, J. Skvarla, M. Uchman, K. Prochazka, B. Angelov, L. Kovacik, V. M. Garamus, C. Mantzaridise and S. Pispas, *Soft Matter*, 2012, **8**, 9412.
2 S. Pispas, *Soft Matter*, 2011, **7**, 474.
3 V. A. Baulin and E. Trizac, *Soft Matter*, 2012, **8**, 6755.
4 M. Kamimura, J. O. Kim, A. V. Kabanov, T. K. Bronich and Y. Nagasaki, *J. Controlled Release*, 2012, **160**, 486.
5 A. Tamura and Y. Nagasaki, *Nanomedicine*, 2010, **5**, 1089.
6 Y. P. Wang, P. Han, H. P. Xu, Z. Q. Wang, X. Zhang and A. V. Kabanov, *Langmuir*, 2010, **26**, 709.
7 N. Bayó-Puxan, M. H. Dufresne, A. E. Felber, B. Castagner and J. C. Leroux, *J. Controlled Release*, 2011, **156**, 118.
8 M. R. Park, C. J. Chun, S. W. Ahn, M. H. Ki, C. S. Cho and S. C. Song, *J. Controlled Release*, 2010, **147**, 359.
9 K. T. Oh, T. K. Bronich, L. Bromberg, T. A. Hatton and A. V. Kabanov, *J. Controlled Release*, 2006, **115**, 9.
10 V. Vergaro, F. Scarlino, C. Bellomo, R. Rinaldi, D. Vergara, M. Maffia, F. Baldassarre, G. Giannellic, X. C. Zhang, Y. M. Lvov and S. Leporatti, *Adv. Drug Delivery Rev.*, 2011, **63**, 847.
11 D. Hernán Pérez de la Ossa, A. Ligresti, M. E. Gil-Alegre, M. R. Aberturas, J. Molpeceres, V. Di Marzo and A. I. Torres Suárez, *J. Controlled Release*, 2012, **161**, 927.
12 C. Y. Gong, Y. J. Wang, X. H. Wang, X. W. Wei, Q. J. Wu, B. L. Wang, P. W. Dong, L. J. Chen, F. Luo and Z. Y. Qian, *J. Nanopart. Res.*, 2011, **13**, 721.
13 P. Zhao, L. X. Liu, X. Q. Feng, C. Wang, X. T. Shuai and Y. M. Chen, *Macromol. Rapid Commun.*, 2012, **33**, 1351.
14 B. Vroman, M. Mazza, M. R. Fernandez, R. Jerome and V. Preat, *J. Controlled Release*, 2007, **118**, 136.
15 J. J. Liu, Y. Zhang, J. L. Yan and M. D. Lang, *J. Mater. Chem.*, 2011, **21**, 6677.
16 W. J. Zhao, B. J. Wang, C. M. Wei, G. Y. Yuan, F. L. Bu and R. C. Guo, *J. Clin. Pharm. Ther.*, 2008, **33**, 289.
17 S. Takeda, K. Ishihara, Y. Wakui, S. Amagaya, M. Maruno, T. Akao and K. Kobashi, *J. Pharm. Pharmacol.*, 1996, **48**, 902.
18 Z. P. John Lin, S. X. Qiu, A. Wufuer and L. Shuma, *J. Chromatogr., B: Anal. Technol. Biomed. Life Sci.*, 2005, **814**, 201.
19 L. Ding, X. Huang, J. Yang, X. J. Bian, Z. X. Zhang and G. Y. Liu, *J. Pharm. Biomed. Anal.*, 2006, **40**, 758.
20 H. Takahashi, H. Onishi and Y. Machida, *J. Pharm. Pharmacol.*, 2004, **56**, 437.
21 C. Marianecci, F. Rinaldi, M. Mastriota, S. Pieretti, E. Trapasso, D. Paolino and M. Carafa, *J. Controlled Release*, 2012, **164**, 17.
22 Y. Wu, W. L. Yang, C. C. Wang, J. H. Hu and S. K. Fu, *Int. J. Pharm.*, 2005, **295**, 235.
23 Y. L. Zheng, Y. Wu, W. L. Yang, C. C. Wang, S. K. Fu and X. Z. Shen, *J. Pharm. Sci.*, 2006, **95**, 181.
24 K. W. Yang, X. R. Li, Z. L. Yang, P. Z. Li, F. Wang and Y. Liu, *J. Biomed. Mater. Res., Part A*, 2008, **88**, 140–148.
25 S. Li, Y. Q. Qiu, S. H. Zhang and Y. H. Gao, *Acta Phys.-Chim. Sin.*, 2011, **27**, 2167.
26 H. Arimura, Y. Ohya and T. Ouchi, *Biomacromolecules*, 2005, **6**, 720.
27 J. L. Yan, Z. Y. Ye, M. Chen, Z. Z. Liu, Y. Xiao, Y. Zhang, Y. Zhou, W. S. Tan and M. D. Lang, *Biomacromolecules*, 2011, **12**, 2562.
28 H. Kudo, T. Takahara, Y. Yata, K. Kawai, W. Zhang and T. Sugiyama, *J. Hepatol.*, 2009, **51**, 168.
29 G. A. Bulla, E. Givens, S. Brown, B. Oladiran and D. Kraus, *J. Cell Sci.*, 2000, **114**, 1205.
30 Y. Wang, Y. J. Ma, B. S. Yang, M. R. Bi and L. Y. Chen, *Chin. J. Hepatol.*, 2005, **13**, 132.
31 H. Guo, A. L. Huang, Y. Q. Yao, N. Tang and D. F. Zhang, *Chin. J. Hepatol.*, 2004, **12**, 159.
32 Y. Gotoh, Y. Ishizuka, T. Mastuura and S. Niimi, *Biomacromolecules*, 2011, **12**, 1532.
33 D. Z. Zhang, H. Ren and D. F. Zhang, *Mod. Med. Health*, 2004, **20**, 597.
34 T. Kuwabara and S. I. Ohmi, *Apoptosis*, 2004, **9**, 467.